--Supporting Information--

Engineering a Large Scale Indium Nanodot Array for Refractive Index Sensing

Xiaoqing Xu,[*,†,‡] Xiaolin Hu,[†] Xiaoshu Chen,[§] Yangsen Kang,[†] Zhiping Zhang,[†] Kokab B. Parizi,[†] H.-S. Philip Wong[*,†]

[†]Department of Electrical Engineering, Stanford University, Stanford, California 94305, United States
[‡]Stanford Nanofabrication Facility, Stanford University, Stanford, California 94305, United States
[§]Department of Electrical and Computer Engineering, University of Minnesota, Minneapolis, Minnesota 55455, United States

Corresponding Authors
*E-mail: steelxu@stanford.edu (X.X.).
*E-mail: hspwong@stanford.edu (H.-S.P.W.).
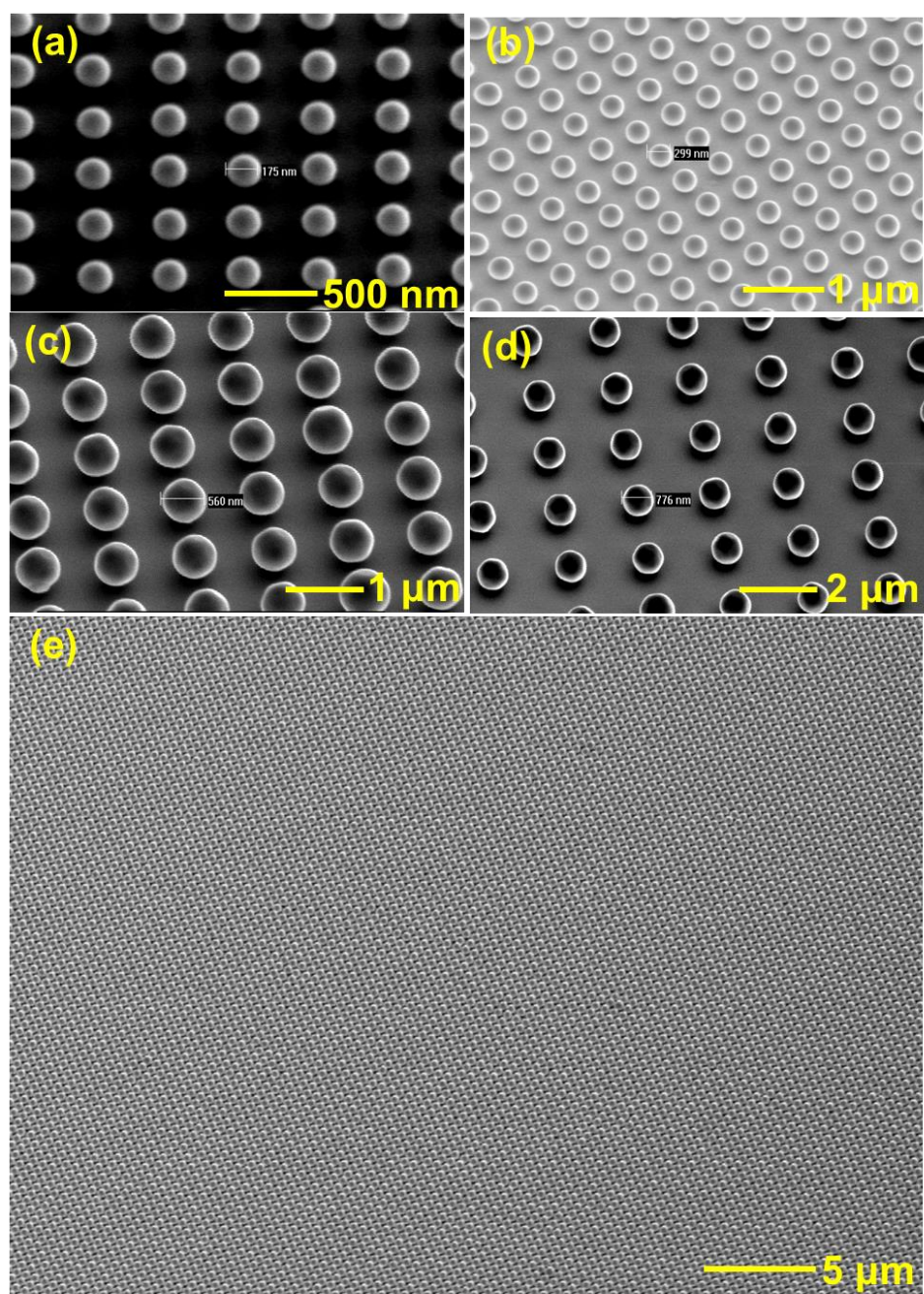
Figure S1

Figure S1. Indium nanodot arrays with different diameters and periods: (a) 175 nm diameter, 400 nm period; (b) 299 nm diameter, 550 nm period; (c) 560 nm diameter, 1 μm period; (d) 776 nm diameter, 2 μm period; (e) Large scale image of indium nanodot array
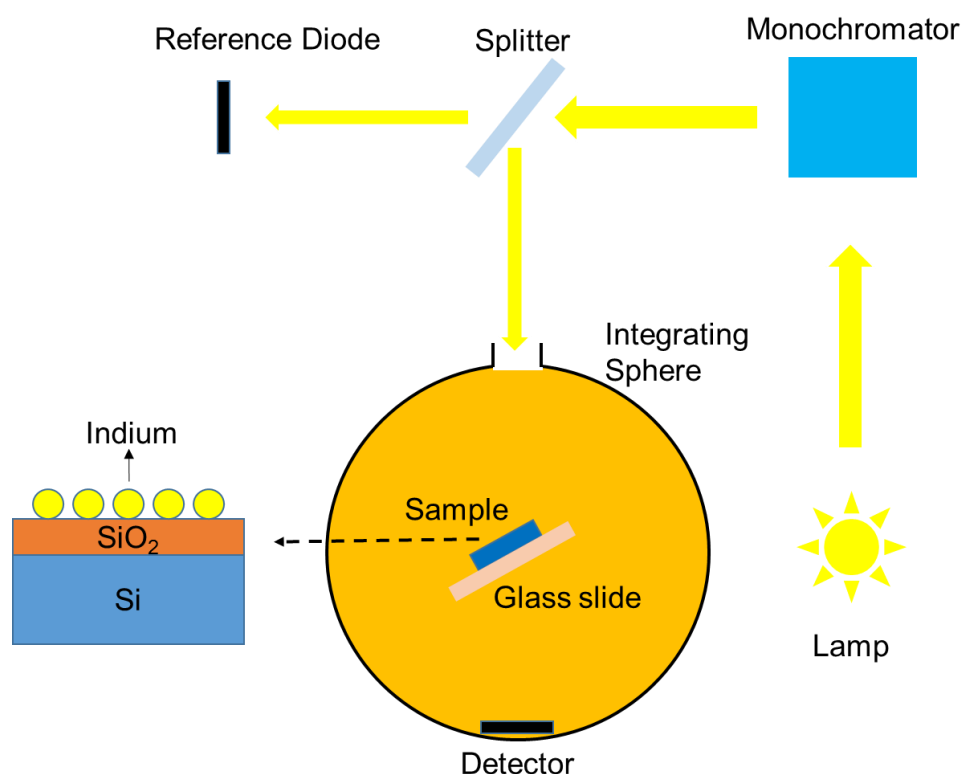
Optical Integrating Sphere setup

Figure S2. The Optical Integrating Sphere setup for reflection measurement

Reflection measurements are taken using an Integrating Sphere system schematically shown in Figure S2. Incident light comes into the sphere through a small port and shines onto the sample mounted at the center of the sphere. The reflection incident angle can be varied from 0° to 90° by tilting the sample stage. The reflected and transmitted light is scattered uniformly by the interior sphere wall. A silicon detector mounted at the back of the sphere reads the photocurrent. The ratio of photocurrent responses, after and before mounting the sample, gives the total amount of reflection and transmission of the sample. Since our nanodot samples have a Si substrate of 500 μm thick with a band edge absorption at 1100 nm, no transmission is expected at the measured wavelength range of 400 nm to 1100 nm. So the signal collected from our sample is reflection only. In order to eliminate the systematic errors due to the possible intensity drift of the light source, a reference diode is used to monitor the light source and compensate for this change.
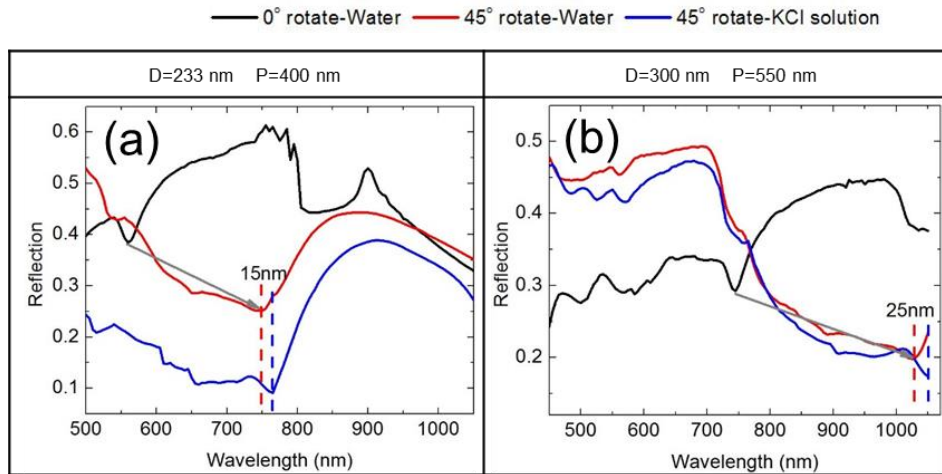
Figure S3

Figure S3. Reflection spectra after 45º in-plane rotation, of an nanodot array with the (a) diameter of 233 nm and period of 400 nm, and (b) diameter of 300 nm and period of 550 nm at the incident angle of 30º
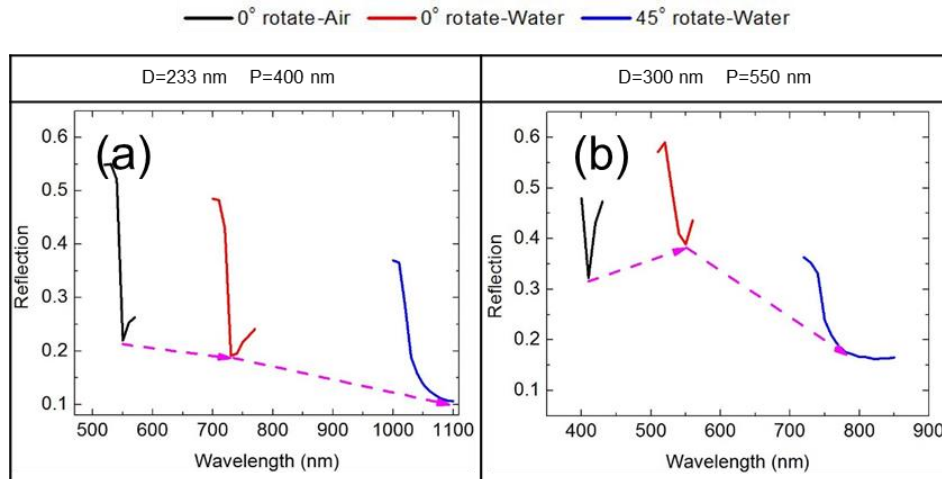
Figure S4

Figure S4. Simulated dip location evolution before and after 45º in-plane rotation, of a nanodot array with the (a) diameter of 233 nm and period of 400 nm, and (b) diameter of 300 nm and period of 550 nm at the incident angle of 30º.

Analysis of the origin of resonance dips by FDTD simulation

To investigate the origin of resonance dips, we compared the simulated reflection spectra of nanodot (ND) only and ND on SiO_2/Si substrate, in both air and water environments, for the ND array with the diameter of 233 nm and period of 400 nm at 60° incidence as an example. As shown in Figure S5, there is a resonance dip at ~520 nm in the case of ND only in air environment, which is dominated by TE component, and it is shifted to ~690 nm in water environment. There are two other dips in water environment, one at ~460 nm as a combined effect of both TE and TM components, and the other at ~590 nm originated from TM component, which do not show up in the simulated wavelength range of 400~800 nm in air due to the detecting wavelength limit of the setup. In the case of ND on substrate, there is also a resonance dip at similar wavelength of ~540 nm but as a combined effect of both TE and TM components in air environment, and it is shifted to ~718 nm in water environment. So adding the SiO_2/Si substrate modified the dip at ~690 nm by contributing to the TM component and then shifted the dip to ~718 nm. Therefore, dip C in Figure S5(d) is a combined effect of the ND and the substrate. The two other dips shown at ~460 nm and ~590 nm respectively in Figure S5(b) also show up at similar wavelengths in Figure S5(d), labeled as dip A and dip B respectively. However, dip A is dominated by TE component in the case of ND on substrate, as compared to a combined effect of TE and TM components in the case of ND only, indicating dip A can be originated solely from the TE component of ND only with the TM component decayed when interacting with the substrate. Dip B, however, is a combined effect of TE and TM components, as compared to TM component only in the case of ND only, so is a combined effect of the ND and the substrate.
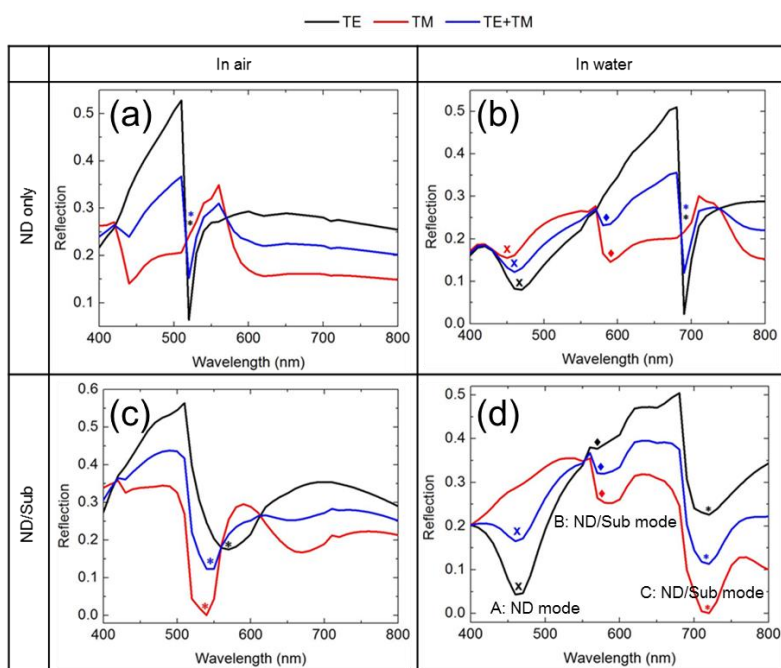

Figure S5. Simulated reflection spectra comparison of ND only (a) in air, (b) in water and ND on substrate (ND/Sub): (c) in air, (d) in water

To further verify the origins of dips A, B and C, we compared the simulated reflection spectra at different ND periods of 400 nm, 450 nm and 550 nm. The relevant dips for each period are labeled in Figure S6. As shown in Figure S6(a), the three dips at 400 nm period, 460 nm, 590 nm, and 718 nm, are shifted to 506 nm, 643 nm, and 790 nm respectively at 450 nm period. The resonance wavelength ratios are all very close to the period ratio of 1.125 (450/400). And in Figure S6(b), the two dips at 400 nm period, 590 nm and 718 nm, are shifted to 790 nm and 940 nm respectively at 550 nm period. Again, the resonance wavelength ratios are all very close to the period ratio of 1.375 (550/400). Therefore, it's concluded that dips A, B and C are all ND periodicity related modes, with dip A being likely from ND mode only, while dips B and C being combined effects of ND and the substrate.
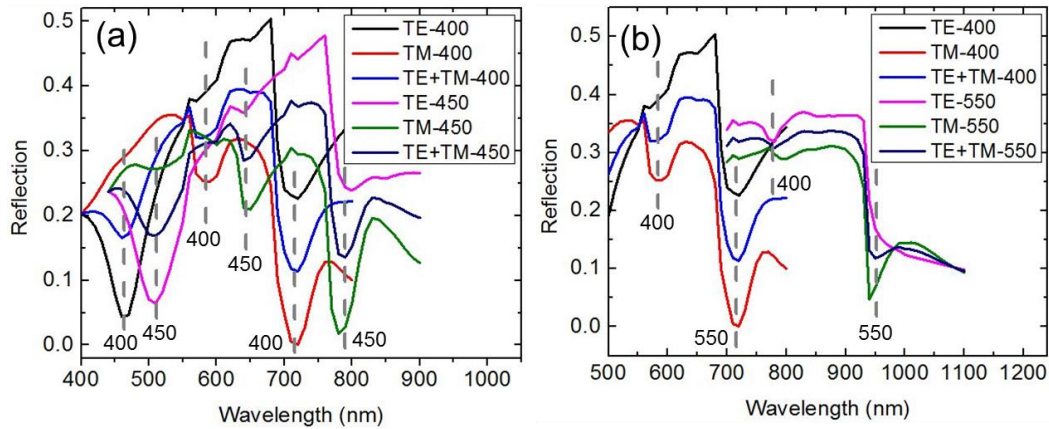

Figure S6. Simulated reflection spectra comparison on ND period variation (a) 400 nm vs 450 nm period, (b) 400 nm vs 550 nm period